Journal Pre-proof

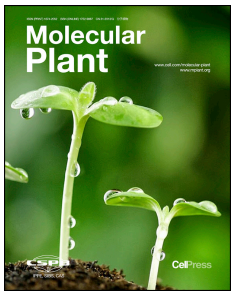

Next-generation mapping of the salicylic acid signaling hub and transcriptional cascade

Jordan Powers, Xing Zhang, Andres V. Reyes, Raul Zavaliev, Roni Ochakovski, Shou-Ling Xu, Xinnian Dong

PII: S1674-2052(24)00263-6

DOI: https://doi.org/10.1016/j.molp.2024.08.008

Reference: MOLP 1777

To appear in: *MOLECULAR PLANT*

Received Date: 1 March 2024

Revised Date: 27 June 2024

Accepted Date: 20 August 2024

Please cite this article as: Powers J., Zhang X., Reyes A.V., Zavaliev R., Ochakovski R., Xu S.-L., and Dong X. (2024). Next-generation mapping of the salicylic acid signaling hub and transcriptional cascade . Mol. Plant. doi: https://doi.org/10.1016/j.molp.2024.08.008.

TITLE

Next-generation mapping of the salicylic acid signaling hub and transcriptional cascade

AUTHORS

Jordan Powers[1,2], Xing Zhang[1], Andres V. Reyes[3], Raul Zavaliev[1,4], Roni Ochakovski[1], Shou-Ling Xu[3], and Xinnian Dong[1,2*]

AFFILIATIONS

[1]Howard Hughes Medical Institute, Duke University, Durham, NC 27708, USA

[2]University Program in Genetics and Genomics, Duke University, Durham, NC 27708, USA

[3]Carnegie Institute for Science, Stanford University, Stanford, CA 94305, USA

[4]Present address: Department of Biology, Brookhaven National Laboratory, Upton, NY 11973, USA

**Correspondence: xdong@duke.edu*

RUNNING TITLE

Mapping the salicylic acid signal hub and cascade

SUMMARY

TurboID and greenCUT&RUN identified the signaling hub components, as biomolecular condensates, in salicylic acid-mediated immune transcription and elucidated the signaling cascade initiated by NPR1 with TGA TFs and executed by WRKY TFs. Globally, the NPR1-signaling hub

is strikingly similar to that of GBPL3 except associated TFs, suggesting that common regulatory modules are recruited to reprogram specific transcriptomes through unique TF-binding.

ABSTRACT

For over 60 years, salicylic acid (SA) has been known as a plant immune signal required for basal and systemic acquired resistance (SAR). SA activates these immune responses by reprogramming ~20% of the transcriptome through the function of NPR1. However, components in the NPR1-signaling hub, which appears as nuclear condensates, and the NPR1-signaling cascade remained elusive due to difficulties in studying this transcriptional cofactor whose chromatin association is indirect and likely transient. To overcome this challenge, we applied TurboID to divulge the NPR1-proxiome, which detected almost all known NPR1-interactors as well as new components of transcription-related complexes. Testing of new components showed that chromatin remodeling and histone demethylation contribute to SA-induced resistance. Globally, NPR1-proxiome shares a striking similarity to GBPL3-proxiome involved in SA synthesis, except associated transcription factors (TFs), suggesting that common regulatory modules are recruited to reprogram specific transcriptomes by transcriptional cofactors, like NPR1, through binding to unique TFs. Stepwise greenCUT&RUN analyses showed that, upon SA-induction, NPR1 initiates the transcriptional cascade primarily through association with TGA TFs to induce expression of secondary TFs, predominantly WRKYs. WRKY54 and WRKY70 then play a major role in inducing immune-output genes without interacting with NPR1 at the chromatin. Moreover, loss of NPR1 condensate formation decreases the protein's chromatin-association and transcriptional activity, indicating the importance of condensates in organizing the NPR1-signaling hub and initiating the transcriptional cascade. This study demonstrates how combinatorial applications of TurboID and stepwise greenCUT&RUN transcend traditional genetic methods to globally map signaling hubs and transcriptional cascades for in-depth explorations.

Keywords: salicylic acid-induced transcription, NPR1, TGA TFs and WRKY TFs, greenCUT&RUN, TurboID, biomolecular condensate

INTRODUCTION

In plants, a local infection can often lead to systemic acquired resistance (SAR) through the accumulation of the phytohormone, salicylic acid (SA) (Malamy et al., 1990; Metraux et al., 1990) which, in *Arabidopsis thaliana*, results in changes of up to 20% of its transcriptome (Wang, Amornsiripanitch and Dong, 2006). This process is mediated by the downstream signal component Nonexpresser of PR genes 1 (NPR1); mutating it leads to a drastic loss of the transcriptional response and enhanced susceptibility to primary and secondary infection (Cao et al., 1994). Further studies have identified NPR1, and its homologs NPR3 and NPR4, as SA receptors in *Arabidopsis* with different binding affinities (Ding et al., 2018; Fu et al., 2012; Kumar et al., 2022; Wang et al., 2020; Wu et al., 2012). Because the NPR1 protein lacks a DNA-binding domain, it was proposed to function as a transcriptional cofactor for transcription factors (TFs), such as TGAs (Despres et al., 2000; Zhang et al., 1999; Zhou et al., 2000) and WRKYs (Chen et al., 2019; Saleh et al., 2015). However, our knowledge of how NPR1 functions molecularly to orchestrate the transcriptome-wide changes in response to SA is still limited by the insufficient sensitivity of current methodologies for investigating a transcriptional cofactor like NPR1. A recent structural study of the NPR1 complex with TGA3 TF showed that NPR1 serves its transcriptional coactivator role as a dimer by bridging two dimeric TGA3 molecules, i.e., $(TGA3)_2$-$(NPR1)_2$-$(TGA3)_2$ (Kumar *et al.*, 2022). The presence of $(NPR1)_2$-$(TGA3)_2$ intermediates in the cryo-EM samples suggests that the NPR1 dimer may function as a platform to nucleate TFs in an enhanceosome. This raises the question, does NPR1 interact with different TFs concurrently in response to SA to activate the

myriad of output genes or, alternatively, initiate the reprogramming through a transcriptional cascade? Besides TFs, NPR1 is likely to be associated with large molecular complexes in response to SA because of the nuclear and cytoplasmic condensates detected for the protein (Saleh *et al.*, 2015; Zavaliev et al., 2020). While the SA-induced NPR1 cytoplasmic condensates (cSINCs) have been characterized (Zavaliev *et al.*, 2020), the contents and function of SA-induced NPR1 nuclear condensates (nSINCs) remain elusive. Therefore, a comprehensive study of NPR1's proximal partners in the nucleus and a stepwise dissection of NPR1 transcriptional targets are essential for elucidating the molecular mechanisms by which this master immune regulator reprograms the transcriptome.

RESULTS

Label-free quantitative analysis of NPR1-proxiome using TurboID identifies core components of gene expression that contribute to SA-induced resistance

To address the question of how the transcriptional reprogramming occurs after the SA-bound NPR1 dimer bridges the TGA TF complexes (Kumar *et al.*, 2022), we generated stable transgenic plants expressing NPR1-3xHA fused with a promiscuous biotin ligase, TurboID (Mair et al., 2019; Xu et al., 2023). The activity of the resulting NPR1-3xHA-TurboID (NPR1-TbID) was validated by its ability to restore, in the *npr1-2* background, the induction of *PR1*, a known NPR1 target (Supplemental Figure 1A). We treated this transgenic line and the control (YFP-YFP-TurboID) with 1 mM SA followed by sample collection at 4 h, when NPR1 displays nuclear accumulation (Kinkema, Fan and Dong, 2000; Zavaliev *et al.*, 2020) and the *PR1* gene expression pattern shows the most rapid increase (Saleh *et al.*, 2015). Samples were then processed under either a mild or a harsh condition (see Methods). Using label-free quantification of the LC-MS/MS

method (Zhu, Smith and Huang, 2010), we identified 234 NPR1-proximal proteins based on their enrichments in the NPR1-3xHA-TurboID sample compared to the control ($FC_{LFQ} \geq 2$, p-value < 0.01 in either condition or p-value < 0.1 in both conditions) (Figure 1A, Supplemental Figure 1B, Supplementary Data 1). To validate our TurboID experiment, we first examined the proximal partners for previously identified NPR1 interactors. We found that, while expressed at a similar level as the negative control protein, NPR1-TbID captured almost all the known NPR1 interactors identified through decades of genetic and molecular studies, including NPR1-like protein 3 (NPR3) and 4 (NPR4) (Fu *et al.*, 2012), NIM1-interacting 1 (NIMIN1) (Weigel, Pfitzner and Gatz, 2005), TGA5 (Despres *et al.*, 2000; Zhang *et al.*, 1999; Zhou *et al.*, 2000), WRKY18 (Chen *et al.*, 2019), histone acetyltransferase of the CBP family 1 (HAC1) (Jin et al., 2018), and components of Mediator (Zhang et al., 2013) (Figure 1B), validating the specificity of the method. Critically, the identified proximal proteins show minimal overlap with the components of cSINCs (Zavaliev *et al.*, 2020) (Figure 1C), giving us confidence that we have identified the nuclear NPR1-proxiome, likely containing components of the NPR1 enhanceosome, instead of cSINCs which form later with higher levels of SA.

This analysis also identified many new NPR1 proximal partners. Gene Ontology (GO) term analysis based on molecular function (MF) demonstrated that these partners are enriched with proteins involved in histone modifications, chromatin remodeling, transcriptional machinery, and splicing complexes (Figure 1D, Supplemental Figure 1C), suggesting involvement of these nuclear functions in reprogramming the SA transcriptome. The multi-functional feature of the NPR1-proxiome is consistent with its central role as a signaling hub for conferring disease resistance against a broad-spectrum of pathogens and abiotic stresses (Olate et al., 2018; Seo, Wi and Park, 2020; Zavaliev *et al.*, 2020).

To validate newly identified NPR1-proximal complexes, we focused on two groups of NPR1 partners: (1) the chromatin remodeling SWItch/Sucrose Non-Fermentable (SWI/SNF) proteins, with BRAHMA (BRM) as a representative, and (2) the histone modifying proteins, with the histone demethylase LSD1-like 3 (LDL3) as a representative. Although chromatin remodeling, nucleosome repositioning, and histone modifications have previously been shown to occur at SA-responsive genes and may play a role in their induction (Jin *et al.*, 2018; Singh et al., 2015), the involvements of BRM and LDL3 have not been tested in SA-induced resistance. We first validated their associations with NPR1 using bimolecular fluorescence complementation (BiFC) in *Nicotiana benthamiana* and observed an SA-dependent increase in the associations between LDL3 or the C-terminus of BRM and NPR1 (Figures 1E and Supplemental Figure 1D). With confirmation of their *in vivo* association, we then performed functional validation of their role in SA-mediated resistance. We found that knocking out the *BRM* and *LDL3* genes partially compromised SA-induced resistance to the bacterial pathogen *Pseudomonas syringae* pv *maculicola* ES4326 (*Psm* ES4326) and complementation using the wild type (WT) *BRM* (in *brm-1*) and *LDL3* genes restored the SA-induced resistance (Figure 1F and 1G, Supplemental Figure 1E and 1F), indicating that chromatin remodeling through BRM and histone demethylation by LDL3 are involved in SA-mediated defense. It is worth noting that given the crucial roles of chromatin remodeling and histone modifications in general transcription regulation, the background effects of the *brm-3, ldl3-1*, and *ldl3-2* mutations had to be taken into consideration by comparing the mutant ± SA data with the WT ± SA data using a 2-way ANOVA. The moderate, yet significant, defense phenotypes of these mutants highlight the efficacy of TurboID in identifying core components of gene expression which are normally difficult to uncover using forward genetic approaches due to their pleiotropic phenotypes or low viability.

Interestingly, both BRM and LDL3 proteins have been reported in proximity to the condensate-forming protein, Guanylate-Binding Protein-Like 3 (GBPL3), which is involved in temperature-sensitive SA synthesis and pathogen response (Huang et al., 2021; Kim et al., 2022; Tang et al., 2022). From an in-depth comparison between the NPR1-proxiome and the GBPL3-proxiome, we discovered a large overlap in transcriptional regulators, chromatin remodelers, and histone modifiers (Figure 1H, shaded in blue). However, most of the TFs appeared to be NPR1-specific partners (19/24). This supports the hypothesis that transcriptome reprogramming is mediated by recruiting common transcriptional regulatory modules and machineries to unique TFs through hub proteins, such as NPR1, which have the intrinsic property to form biomolecular condensates (Mann and Notani, 2023).

QuantSeq shows WRKY54 and WRKY70 are positive regulators of SA/NPR1-mediated transcriptional reprogramming.

NPR1 is known to interact with several different TFs and TF families, including TGAs, WRKYs, TCPs, MYCs, HSFs, and EIN3 (Huang et al., 2020; Li et al., 2018; Nomoto et al., 2021; Olate *et al.*, 2018; Saleh *et al.*, 2015; Zhang *et al.*, 1999). Among the TFs unique to NPR1 based on our TurboID data, TGA and WRKY TFs have been observed in multiple studies to interact with NPR1 in response to SA (Chen *et al.*, 2019; Despres *et al.*, 2000; Saleh *et al.*, 2015; Zavaliev *et al.*, 2020; Zhang *et al.*, 1999; Zhou *et al.*, 2000) (Figure 1B and 1H). While TGA3 TF has been shown to bind DNA in complex with NPR1 in the cryo-EM structure (Kumar *et al.*, 2022), the transcriptional role of WRKY TFs and their relationship with NPR1 in SA-mediated gene expression is less straightforward. WRKYs constitute a diverse TF family whose own expression is dynamically induced upon stress, displaying functional redundancies as well as distinct roles in

gene expression regulation (Kalde et al., 2003; Wang, Amornsiripanitch and Dong, 2006; Xu et al., 2006). In this study, we focused on WRKY70 and its closest homolog WRKY54 (WRKY54/70) because, although WRKY70 has been shown to associate with NPR1, its single mutant exhibits minimal transcriptional differences compared to WT plants (Saleh *et al.*, 2015). We performed QuantSeq (Moll et al., 2014) on WT, *npr1-2*, and the *wrky54 wrky70* (*wrky54/70*) double mutant 8 h after SA induction. Principal component analysis (PCA) demonstrated a separation of WT treated with SA from all other samples (Supplemental Figure 2A), indicating that both *npr1-2* and *wrky54/70* exhibit abnormal responses to SA compared to WT. In WT, we identified 3528 differentially expressed genes in response to SA, whereas, only 722 and 532 in *npr1-2* and *wrky54/70*, respectively ($|\log_2 \text{foldchange}| \geq 1$, adjusted p-value < 0.1) (Supplemental Figure 2B - 2D and Supplementary Data 2). Furthermore, both mutants displayed few differentially expressed genes basally compared to WT (Supplemental Figure 2E and 2F), indicating the loss of induction by SA in the mutants is not due to variations in their background gene expression. Among the 1909 SA-induced genes, 1022 were NPR1-dependent and 804 were WRKY54/70-dependent (Supplemental Figure 2G, Supplementary Data 2), and the global transcriptome displayed a higher degree of correlation with NPR1 than with WRKY54/70 (Supplemental Figure 2H and 2I). GO term analyses of NPR1- and/or WRKY-dependent genes did not provide further resolution, with similar enrichments for defense response and SA-related processes (Supplemental Figure 3A - 3C). Interestingly, promoter examination of these genes led to the detection of the WRKY-binding "W-box" as the most enriched motif (Supplemental Figure 3D - 3F), instead of the *as-1* element for TGA TFs, even for those NPR1-dependent, WRKY54/70-independent genes (Supplemental Figure 3F), suggesting that WRKY TFs are the major TFs responsible for the SA-mediated transcriptional output.

Genome-wide greenCUT&RUN identifies WRKY TF genes as a major group of NPR1 transcriptional targets

The enrichment of the W-box in our QuantSeq data (Supplemental Figure 3D-3F) and in other transcriptome profiling datasets at various time points after SA or SA analog treatment (Ding *et al.*, 2018; Jin *et al.*, 2018; Maleck et al., 2000; Wang, Amornsiripanitch and Dong, 2006) (Supplemental Figure 3G-3I) raised the question about the role of TGA TFs in the SA signaling cascade and the relationship between TGA or WRKY TFs and NPR1. To address these questions, we performed Cleavage Under Target and Release Using Nuclease (CUT&RUN) followed by next-generation sequencing (Skene and Henikoff, 2017) on *35S:NPR1-GFP* and *35S:GFP* transgenic plants 4 h after SA induction to identify direct transcriptional targets of NPR1, utilizing an anti-GFP antibody. Since CUT&RUN does not require crosslinking, it offers a major advantage over the traditional chromatin immunoprecipitation-sequencing (ChIP-seq) methods by reducing false positives introduced by cross-linking and allowing identification of loci bound by protein of interest in the native chromatin state (Meers et al., 2019). Unfortunately, the experiment failed to detect any differential peaks between NPR1-GFP and GFP samples with minimal difference seen at either known NPR1 targets or globally (Supplemental Figure 4A-4D). This suggests that while CUT&RUN has significantly enhanced sensitivity for identifying TFs that interact directly with chromatin (Meers, Janssens and Henikoff, 2019) and histone modifications (Zheng and Gehring, 2019), an even more sensitive methodology is required for detecting targets of transcriptional cofactors, like NPR1, whose proximity to DNA depends on its interaction with TFs.

To further improve the sensitivity of the CUT&RUN methodology, which relies on transient interactions of multiple proteins that ultimately lead to the cutting and release of target

DNA sequences by pA-MNase, we adopted an anti-GFP nanobody-based CUT&RUN approach, 'greenCUT&RUN', where a GFP-specific nanobody is fused directly to the MNase (Koidl and Timmers, 2021). Similar to CUT&RUN, greenCUT&RUN also allows profiling of the chromatin in the native state to reduce the number of false positives (Nizamuddin et al., 2021). In contrast to the initial CUT&RUN data (Supplemental Figure 4A-4D), the new method led to a clear separation of the SA-treated NPR1-GFP samples from both the untreated NPR1-GFP and the GFP samples (Figure 2A). Further demonstrating the success of our greenCUT&RUN experiment, PCA showed a clear clustering of SA-treated NPR1 samples separated from all other samples (Supplemental Figure 4E). Based on the three NPR1-GFP replicates, we were able to detect 385 reproducible NPR1-GFP-specific peaks (Supplemental Figure 4F, Supplementary Data 3). Furthermore, by examining the promoter of the known NPR1 target gene, *PR1*, an SA-dependent accumulation of NPR1-GFP could clearly be observed compared to the GFP input (Figure 2B). By averaging the global alignment of the binding loci, we detected a significant enrichment of NPR1-GFP at the promoters of its target genes upon SA treatment compared to the untreated samples (Figure 2C). Among these loci, 84.2% occurred upstream of the transcriptional start site (TSS). Interestingly, the distances from TSS of these binding peaks varied widely from gene to gene, ranging from immediately before the TSS to several thousand base pairs (kb) upstream, with only 53% within 1 kb from TSS (Supplemental Figure 4G). These results are consistent with the proposed function of NPR1 in organizing an enhanceosome by bridging distal binding sites through DNA looping and interacting with larger transcriptional machineries like the SWI/SNF complex and Mediator (Bazett-Jones et al., 1999; Kagey et al., 2010) (Figure 1H).

Among the NPR1 peaks, we detected the TGA-binding *as-1* element, TGACG, as the most significantly enriched motif (Figure 2D). While there was an increased cutting frequency by the

MNase near the motif, the motif itself was protected, further supporting the notion that NPR1 binds to the DNA through TGA TFs (Figure 2E). Additionally, we also detected enrichment of Teosinte branched 1/Cycloidea/Proliferating cell factors (TCP) and Cycling Dof Factor (CDF) binding motifs (Figure 2E), which are two other TFs detected in our TurboID experiment (Figure 1H). Further supporting the TGA binding motif being the most enriched NPR1 loci, analysis of previously published DNA Affinity Purification Sequencing (DAP-seq) data (O'Malley et al., 2016) demonstrated that TGA5 binds to the same region as NPR1 (Supplemental Figure 5). As expected, the NPR1-target genes are largely related to defense response and cross-talk between SA and another plant defense hormone, jasmonic acid (JA) (Figure 2F).

The reduced sequencing depth needed for greenCUT&RUN allowed us to perform a time course on NPR1-GFP in response to SA. Analysis of the data detected many shared targets at all time points (Figure 2G). Interestingly, these shared peaks (97 loci) displayed stronger chromatin binding compared to the time point-specific peaks (Figure 2H). To compare methods, we then examined our greenCUT&RUN data 8 hours after SA treatment with a recently reported NPR1 ChIP-seq performed after treatment with the synthetic analog of SA, 2,6-dichloroisonicotinic acid (INA), for 10 hours followed by a mild or harsh chromatin isolation protocol (Yun et al., 2024). We observe 207 overlapping peaks between our greenCUT&RUN and both ChIP-seq conditions (Supplemental Figure 6A). The majority of unique peaks were observed in the mildly processed ChIP-seq (“mild-specific”) (Supplemental Figure 6A). While motif analysis of all samples showed enrichment of the *as-1* element (Supplemental Figure 6B-6D), the GO term analysis displayed striking differences, with the shared peaks enriched with defense-related biological processes (Supplemental Figure 6E), while the mild-specific peaks from ChIP-seq were largely enriched in response to other stresses (Supplemental Figure 6F). This is in contrast to the greenCUT&RUN-

specific peaks which still had GO terms related to SA signaling and defense (Supplementary Figure 6G). We hypothesize that these mild-specific signals in ChIP-seq may result from the crosslinking step, which could capture transient interactions between NPR1 and TGA, when NPR1 scans the chromosome, instead of those more stable and transcriptionally active TGA_2-$NPR1_2$-TGA_2 enhanceosome complex (Kumar *et al.*, 2022).

Interestingly, NPR1 does not display enrichment of the W-box at any time after SA treatment (Supplemental Figure 7A). Furthermore, greenCUT&RUN on the NPR1 SUMO-deficient mutant, $npr1^{sim3}$ (sim3), which preferentially interacts with WRKY70 (Saleh *et al.*, 2015), showed minimal binding at NPR1 loci (Figure 2I) with no enriched motifs. Taken together, these results indicate that NPR1 is associated with TGA TFs, but not WRKYs, during the course of SA induction. Moreover, compared to the thousands of differentially expressed genes in response to SA, there were only a few hundred NPR1-target genes. These data suggest that NPR1 reprograms the transcriptome through multiple steps, instead of through parallel association with multiple TFs. In support of this hypothesis, the GO terms of NPR1 transcriptional targets are largely enriched with TFs and other DNA-binding proteins (Figure 2F). Analysis of the genes annotated as DNA binding and/or cis-regulatory binding detected four major TF families: WRKYs, NACs, ERFs, and MYBs, with WRKYs representing the largest family (Supplemental Figure 7B). Of note, NPR1 preferentially targets group III WRKY TFs, including WRKY70 (Supplemental Figure 7C and 7D), suggesting their involvement in further propagating SA-induced gene expression.

Genome-wide greenCUT&RUN establishes WRKY70 as a downstream TF in the SA-induced transcriptional cascade

To examine the role of group III WRKYs in SA/NPR1-mediated reprogramming of the immune transcriptome, we performed a subsequent greenCUT&RUN analysis on *35S:WRKY70*, the most abundantly expressed *WRKY* in WT after SA treatment (Supplementary Data 2). Previously, WRKY70 was hypothesized to be removed from the *PR1* promoter by NPR1 in response to SA (Saleh *et al.*, 2015). To consider this hypothesis, we collected samples 2 h after SA treatment. Similar to our NPR1-GFP greenCUT&RUN experiment, we found that WRKY70-GFP samples were well-correlated with one another, while distinguished from those of the GFP samples (Supplemental Figure 8A and 8B). Surprisingly, they were also distinct from the NPR1-GFP greenCUT&RUN data (Supplemental Figure 8A and 8B). From this experiment, we detected 1477 reproducible WRKY70-GFP-specific peaks (Supplemental Figure 8C, Supplementary Data 4). It was evident that the WRKY70-GFP samples had a higher percentage of reproducible peaks (43.4% - 61.3%) compared to those in the NPR1-GFP samples (33.1% - 36.3%) (Supplemental Figures 4F and 8C), consistent with WRKY70 being a TF binding directly to DNA. Examining all target genes showed that WRKY70, like NPR1, was mainly detected at the promoters of its target genes with only 14.4% of WRKY70 >1 kb upstream of TSS compared to the 31.2% for NPR1 (Figure 3A, Supplemental Figures 4G and 8D). As expected, a high enrichment of W-box was observed in these WRKY70-bound loci (Figure 3B). Interestingly, while defense-related biological processes were still the top enrichments in the WRKY-target genes, they differ from those of NPR1-target genes in their molecular functions (MF). Where NPR1 targets TF genes, WRKY70 targets those involved in ADP-binding (mostly encoding nucleotide-binding domain and leucine-rich repeat-containing immune receptors, NB-LRRs), calmodulin-binding, and kinase activity (Figure 3C), implying that WRKY70, whose transcription is induced by NPR1-TGA (Wang, Amornsiripanitch and Dong, 2006) (Supplementary Data 2), is involved in the downstream events

in the signaling cascade of NPR1-mediated transcriptional reprogramming. Furthermore, these genes were highly correlated to those transcriptionally impaired in the *wrky54/70* mutant (Supplemental Figure 8E), with ~49% (522/1067) of WRKY70 targets with detectable expression being differentially expressed in response to SA and ~68% (355/522) displaying differential expression dependency on WRKY54/70 (Supplementary Data 2 and 4), demonstrating they are true WRKY70 targets.

Apart from these distinct transcriptional targets, there were a smaller number of shared target genes between WRKY70 (116/1476) and NPR1 (116/346) (Fig. 3D), suggesting a possible interplay between WRKY70 and NPR1 in regulating the transcription of these genes. However, in two common target promoters examined, we detected WRKY70 and NPR1 at distinct loci from one another (Figure 3E and 3F). Interestingly, *PR1* was not even detected in our WRKY70-GFP samples, despite the negative regulation WRKY70 has on the transcript (Li, Zhong and Palva, 2017). To further examine the relationship between NPR1 and WRKY70, we examined the peak patterns at all the shared target gene promoters. As expected, NPR1 samples showed one distinct peak (Figure 3G), typical of its global target profile (Figure 3H), while WRKY70 samples were not confined to the defined peak region of NPR1, displaying binding near but not in the peak region (Figure 3G), which is atypical for its own global target profile, where WRKY70 binding is confined within the peak region (Figure 3H). These data further demonstrate that NPR1 is unlikely to switch associations between WRKY and TGA TFs at the chromatin level as previously proposed (Saleh *et al.*, 2015). Instead, NPR1 has been found to interact with WRKY70 in cSINCs to sequester and degrade WRKY70 (Zavaliev *et al.*, 2020). Nevertheless, the shared gene targets of NPR1 and WRKY70 with distinct loci suggest a possible regulatory dependence on both proteins.

The sequential NPR1- and WRKY70-greenCUT&RUN analyses elucidated an SA-signaling cascade in which the SA-activated NPR1 induces the expression of *WRKY* TF genes through association with TGA TFs. Consistently, by comparing our QuantSeq results with NPR1- and WRKY70-greenCUT&RUN targets, we found that, while NPR1 had the expected strong regulation of WRKY70-target genes (r = 0.85) (Figure 3I), WRKY54 and WRKY70 had a more moderate correlation with NPR1-targets (r = 0.69) (Figure 3J), demonstrating that WRKY54/70 targets are regulated by NPR1, while NPR1 targets are also regulated by WRKY54/70, likely through a feedback loop. Taken together, these results suggest that WRKY54 and WRKY70 are predominantly positive TFs of SA-mediated gene transcription, in addition to their role as feedback repressors of SA synthesis (Wang, Amornsiripanitch and Dong, 2006). This hypothesis is further supported by the compromised SA-mediated resistance to *Psm* ES4326 observed in the *wrky54/70* double mutant compared to WT (Figure 3K).

SA-induced condensate formation of NPR1 promotes its chromatin binding and transcriptional activity

With the identification of NPR1 proximal partners and direct transcriptional targets in the signaling cascade, we then tested our hypothesis that SA-induced condensate formation is critical for NPR1 to organize the enhanceosome to initiate transcription. We first performed greenCUT&RUN in a transgenic line expressing the npr1^{rdr3}-GFP protein (referred to as rdr3) (Zavaliev *et al.*, 2020), which accumulates to high levels in the nucleus upon SA induction, but fails to form either nuclear or cytoplasmic condensates (Zavaliev *et al.*, 2020). We found that chromatin association of rdr3 occurred at the same loci as the WT NPR1 in an SA-dependent manner, but at a significantly lower affinity (Figure 4A), even though the mutant protein has a

higher-than-WT nuclear distribution (Zavaliev *et al.*, 2020). Interestingly, the reduced rdr3 binding to the TGA TFs was only observed *in planta* (Figure 4B - 4D), not in the yeast two-hybrid assay (Figure 4E), suggesting that the decreased rdr3 chromatin association is less likely due to its diminished binding to TGA TFs than the reduced stability of its complex with TGA TFs due to inability to form the nuclear condensates. Moreover, despite of elevated protein amounts and comparable transcript levels (Figure 4F and 4G), rdr3 exhibited significantly compromised activity in inducing direct target genes, *PR1*, *WRKY18*, and *WRKY70* (Figure 4H - 4J) compared to the WT NPR1-GFP control, supporting our hypothesis that NPR1 orchestrates the transcriptomic changes upon SA-induction by forming biomolecular condensates.

BRM association with NPR1 and WRKY70 targets are enhanced upon SA treatment

Our TurboID experiment identified BRM in the NPR1 nuclear proxiome (Figure 1H) and loss of BRM resulted in compromised SA-induced resistance (Figure 1F, Supplemental Figure 1E). However, due to the essential role that BRM plays in transcription, it is unclear whether its proximity to NPR1 is a specific mechanism for activating NPR1-target genes. To address this question, we performed greenCUT&RUN on *BRM:BRM-GFP* transgenic plants (Li et al., 2016) treated with 1 mM SA or H_2O for 4 h. Interestingly, we found that the overall BRM accumulation stayed constant under both mock and SA-induced conditions at BRM-specific peaks, indicating that SA has minimal impact on the general BRM binding to the chromatin (Figure 4K, Supplementary Data 5). However, in agreement with our TurboID and BiFC data (Fig. 1E and 1H), we observed an increase in BRM accumulation at NPR1 loci upon SA treatment (Figure 4L). Interestingly, we also detected a similar increase at WRKY70 loci (Figure 4M), indicating that BRM is present at these loci, not as a signaling mechanism, but as a component of the common

transcriptional machinery. Consistent with this hypothesis, increased levels of BRM were also observed at SA-induced genes upon SA treatment (Figure 4N). It would be interesting to examine other regulatory hubs to see if they also have similar proteins in their proximity, thus allowing comprehensive mapping of general transcriptional machinery.

DISCUSSION

By combinatorial applications of label-free quantification of TurboID-based LC-MS/MS data and the greenCUT&RUN technology, the first time in plants, we have transcended decades of molecular genetic studies to generate a comprehensive map of the NPR1-centered transcriptional reprogramming machineries and the transcriptional cascade in response to SA induction (Figure 4O). The validation of the new NPR1 proximal partners (Figure 1E - 1G, Supplemental Figure 1E and 1F) clearly demonstrates the effectiveness of the methodology in identifying signaling hubs formed by proteins, like NPR1, in association with regulatory modules involved in common nuclear functions, such as chromatin remodeling, histone modifications, Mediator, and RNA splicing that also play roles in other stress responses. The robustness of these essential cellular machineries makes it difficult to discern their contributions to specific biological processes through genetic studies. Indeed, the NPR1-proxiome shows high similarity to the GBPL3-proxiome (Tang *et al.*, 2022), with the major distinction in their associated TFs (Figure 1H). Since both the GBPL3-proxiome involved in inducing SA synthesis upon stress (Kim *et al.*, 2022) and the NPR1-proxiome responsible for SA-mediated transcriptional reprogramming can form detectable nuclear biomolecular condensates when overexpressed (Huang *et al.*, 2021; Saleh *et al.*, 2015), it is tempting to hypothesize that in the nucleus, a similar set of transcriptional regulatory modules are recruited to form supramolecular complexes/condensates by distinct

regulators, like NPR1, whose association with unique TFs provides the complexes/condensates functional specificity (Figures 1H and 4O). Furthermore, condensate formation facilitates NPR1's association with the chromatin, as well as target gene induction (Figure 4A - 4J), supporting the notion that SA-induced nuclear NPR1-condensates, i.e., nSINCs, are transcriptionally active.

More experiments are required to demonstrate that NPR1 condensate formation is required for the recruitment of the transcriptional regulatory modules identified in the NPR1-proxiome (Figure 1A, Supplemental Figure 1B, Supplementary Data 1). Though the BRM greenCUT&RUN showed an increase in association to NPR1 loci upon SA induction, significant basal signal was detected in the absence of SA (Figures 1E and 4L), indicating that the association of BRM to NPR1 loci is unlikely SA-dependent, but rather SA-stabilized. It would be exciting to explore which proteins of these transcriptional modules are constitutively present at the promoters and which are recruited in response to induction to initiate transcription. Consistent with NPR1 condensate formation being a dynamic process, SA/NPR1-induced WRKYs as well as several known negative regulators of SA-mediated gene expression, such as NPR3, NPR4, NIMINs, and TPLs, were found to be in the NPR1-proxiome. However, we cannot rule out the possibility that the NPR1-proxiome consists of multiple distinct NPR1-protein complexes or represents responses in different subcellular compartments or leaf cell types (Delannoy et al., 2023; Nobori et al., 2023; Zhu et al., 2023). Future research will be required to understand the dynamics of the NPR1 signaling hub.

The advantage of the greenCUT&RUN method in detecting dynamic chromatin association in the native state is critical for avoiding false positives in identifying true targets of a regulator, like NPR1, which must scan the chromatin to find its partners for a productive binding (Kumar *et al.*, 2022). The ~10 fold-increase in sensitivity compared to ChIP-seq and the ease of the greenCUT&RUN method make time-course experiment feasible, which, in this study,

identified not only the direct NPR1 targets, but also the hierarchical relationship between TGA and WRKY TFs, demonstrating its great potential in dissecting transcriptional cascades. The method has also been shown to be effective in studying dynamic TFs, like WRKY54/70, which play a positive role in SA signaling (Figure 3), in addition to their negative role in SA synthesis reported in our previous study (Wang, Amornsiripanitch and Dong, 2006). The requirement of WRKY54/70 for SA-mediated defense and gene expression discovered in this genome-wide study serendipitously solved the puzzle of why the high levels of SA in the *wrky54/70* double mutant do not lead to *PR* gene induction or enhanced disease resistance (Wang, Amornsiripanitch and Dong, 2006) (Figure 4O).

The SA-responsive transcription factor hierarchy unveiled through the stepwise greenCUT&RUN was previously obscured in the transcriptomic data. As demonstrated in our QuantSeq experiments, statistical analyses of such data failed to detect the initiation step of the SA signaling cascade mediated by NPR1/TGA due to the overwhelming number of WRKY-mediated transcriptional targets induced in the subsequent step of the cascade. Moreover, transcriptomic studies of TF gene families often rely on the usage of available TF knockdown lines or knockout mutants, which either have weak phenotypes due to functional redundancy or pleiotropic defects when higher-order mutants are used. These limitations can now be overcome by the greenCUT&RUN method, which is readily applicable for studying not only TFs, but also proteins with indirect chromatin association.

METHODS

Plant material and growth conditions

All plants used in this study were grown on soil (ProMix B) under 12-h light/12-h dark conditions. The *35S:YFP-YFP-TbID* line was generously gifted by Dr. Zhi-Yong Wang (Carnegie Institution for Sciences) (Kim et al., 2023). The *35S:NPR1-3xHA-TbID* and *35S:npr1^{rdr3}-GFP* constructs were made using Gateway cloning (Thermo Fisher Scientific). *35S:NPR1-3xHA-TbID* was transformed into the *npr1-2* plants using the floral dip method (Clough and Bent, 1998). The *brm-3* (SALK_088462) and *ldl3-2* (SALK_146733) mutants were obtained from ABRC. The *35S:NPR1-GFP*, *35S:npr1^{rdr3}-GFP*, and *35S:WRKY70-GFP* transgenic lines and the *wrky54 wrky70* double mutant were previously described (Wang, Amornsiripanitch and Dong, 2006; Zavaliev *et al.*, 2020). The *BRM:BRM-GFP* line was a generous gift from Dr. Chenlong Li (Sun Yat-sen University) (Li *et al.*, 2016). The *LDL3:LDL3-3xFLAG* and *ldl3-1* lines were generous gifts from Dr. Tetsuji Katutani (University of Tokyo) (Mori et al., 2023).

RNA isolation and qPCR

Total RNA was extracted from 3-week-old plants treated with 1 mM SA or H_2O using Trizol (Rio et al., 2010) (Thermo Fisher Scientific). DNase-treated total RNA was then used for SuperScriptIII Reverse Transcription (Thermo Fisher Scientific). The resulting cDNA samples were diluted tenfold for qPCR reactions using SYBR Green Master Mix to detect transcript levels.

Affinity purification of biotinylated proteins

Affinity purification of biotinylated proteins was performed as previously described (Mair *et al.*, 2019), with minor modifications. Briefly, three replicates (4 g/sample) of 3-week-old plants treated first with 1 mM SA and, 1 h later, with 50 μM biotin for 3 h, were collected, flash frozen, and stored at -80 °C. Samples were ground to a fine powder, dissolved in 4 mL of the extraction

buffer (50 mM Tris-HCl pH 7.5, 150 mM NaCl, 0.1% SDS, 1% NP-40, 0.5% Na-deoxycholate, 1 mM EGTA, 1 mM DTT, and the protease inhibitor cocktail), filtered, and sonicated. Sonicated samples were centrifuged, and biotin was removed from the resulting protein solution using PD-10 desalting columns (GE-Healthcare). The flow-through was collected and subjected to affinity purification using the streptavidin bead (Thermo Fisher Scientific). The resulting samples on the streptavidin beads were processed under two conditions: harsh and mild. The harsh condition involved washing the beads 2x with the extraction buffer, 1x with 1 M KCl, 1x with 100 mM Na_2CO_3, 1x with 2 M Urea in 10 mM Tris-HCl pH 8, and 2x again with the extraction buffer. The mild condition involved washing the beads 7x with the extraction buffer. The processed beads from both conditions were resuspended in 1 mL of the extraction buffer for further processing. Prior to trypsin digestion, the beads underwent further washes. The bead samples corresponding to the harsh conditions were followed by harsh washes consisting of 1x with cold 1 M KCl, 1x with 2 M Urea in 10 mM Tris-HCl pH 8, 2x with cold 50 mM Tris-HCl pH 7.5, and 2x with the Urea wash buffer (50 mM Tris-HCl pH 7.5, 1 M Urea). The bead samples corresponding to the mild conditions were followed by mild washes consisting of 7x with the PBS buffer. Both sample sets were subjected to a 3 h incubation in 80 µl Trypsin buffer (50 mM Tris-HCl pH 7.5, 1 M Urea, 1 mM DTT, and 0.4 µg Trypsin) at 25 °C. The supernatants from the tryptic digest were transferred to new tubes and the beads were washed 2x with 60 µl 1 M Urea in 50 mM Tris-HCl pH 7.5. The combined 200 µL elutes were reduced (final concentration of 4 mM DTT), alkylated (final concentration of 10 mM Iodoacetamide), and digested overnight with 0.5 µg Trypsin. Additional 0.5 µg of trypsin was added in the next morning followed by acidification 4 h later by adding formic acid to a final concentration of ~ 1 % and desalting using OMIX C18 pipette tips (A57003100).

LC-MS/MS

LC-MS/MS was carried out on a Q-Exactive HF hybrid quadrupole-Orbitrap mass spectrometer (Thermo Fisher Scientific), equipped with an Easy LC 1200 UPLC liquid chromatography system (Thermo Fisher Scientific). Peptides were first trapped using a trapping column (Acclaim PepMap 100 C18 HPLC, 75 μm particle size, 2 cm bed length), then separated using analytical column AUR2-25075C18A, 25CM Aurora Series Emitter Column (25 cm x 75 μm, 1.6 μm C18) (IonOpticks). The flow rate was 300 nL/min, and a 120-min gradient was used. Peptides were eluted by a gradient from 3 to 28% solvent B (80% acetonitrile, 0.1% formic acid) over 100 min and from 28 to 44% solvent B over 20 min, followed by a 10 min wash at 90% solvent B. Precursor scan was from mass-to-charge ratio (m/z) 375 to 1,600 and top 20 most intense multiply charged precursors were selected for fragmentation. Peptides were fragmented with higher-energy collision dissociation (HCD) with normalized collision energy (NCE) 27.

Proteomic analysis

Harsh and mild sets of LC-MS/MS spectra were searched separately against the Araport11 database (20220914 version containing 49,467 entries) using the MSFragger 3.2 (Kong et al., 2017) software under default criteria to obtain maximum Label Free Quantification (LFQ) intensities. The search results were analyzed separately in Perseus (Tyanova et al., 2016) (version 1.6.15.0). The processing in Perseus was as follows: MaxLFQ intensities were log2 transformed. Only proteins that had at least two valid values in at least one group (NPR1-TbID or YFP-YFP-TbID) were kept. The remaining missing MaxLFQ intensities were then imputed from a normal distribution that is downshifted by 1.8 and a width of 0.3 column wise. A two-sample t-

test was conducted with a permutation-based (n = 250) FDR = 0.01 and the S0 = 2. Significant NPR1 proximal partners were identified by the following criteria: (1) a p-value < 0.1 in both processing conditions and a $NPR1_{LFQ}/YFP_{LFQ} \geq 2$ or (2) a p-value < 0.01 in either processing condition and a $NPR1_{LFQ}/YFP_{LFQ} \geq 2$. GO Term Analysis was performed using PANTHER(Mi et al., 2013). The interaction network was performed using STRING (Szklarczyk et al., 2019). Plots were generated with ggplot2 (Wickham, 2016), Cytoscape (Shannon et al., 2003), and SRplot.

Bimolecular fluorescence complementation (BiFC) and analysis

Agrobacterium GV3101 carrying indicated constructs were resuspended to $OD_{600\ nm}$ = 0.2 and $OD_{600\ nm}$ = 0.8, for HTB1-mCherry and BiFC constructs, respectively, in acetosyringone-containing water (200 μM) before infiltrating the fully expanded *Nicotiana benthamiana* leaves. After 36 h, the leaves were treated with water (Mock) or 1 mM SA for 8 h followed by confocal imaging on Zeiss 880 Airyscan inverted confocal laser scanning microscope. 488 nm argon laser was used to excite YFP signal with a 516-544 nm emission filter and 561 nm DPSS laser was used to excite mCherry signal with a 592-629 nm emission filter. Region of interest (ROI) manager and BiFC intensities were measured using ImageJ (Schneider, Rasband and Eliceiri, 2012).

SA-induced resistance against bacterial infection

SA-induced resistance was measured as previously described (Liu et al., 2015). Briefly, *Pseudomonas syringae* pv. *maculicola* ES4326 (*Psm* ES4326) was grown at 30 °C on plates containing the King's B medium (KB) for 48 h before resuspended in 10 mM $MgCl_2$. 3-week-old plants were pretreated with 1 mM SA or H_2O for 24 h prior to infection with *Psm* ES4326 at $OD_{600\ nm}$ = 0.001. Leaf discs from 8 infected plants were collected 2 days (for *wrky54 wrky70*) or 3 days

(for *brm-3*, *BRM:BRM-GFP*, *ldl3-1*, *ldl3-2*, and *LDL3:LDL3-3xFLAG*) post infection and individually ground in 0.5 mL of 10 mM $MgCl_2$, serially diluted, and plated on the KB medium supplemented with 100 μg/mL of streptomycin. Colonies were counted two days later.

QuantSeq and data analysis

Total RNA was extracted from 3-week-old leaves treated with 1 mM SA or H_2O for 8 h using Split RNA Extraction Kit (Lexogen GmbH). RNA concentration was measured with Qubit RNA BR assay (Thermo Fisher Scientific) and integrity was checked with Agilent 2100 Bioanalyzer. Approximately 400 ng of RNA was used for library construction using the QuantSeq 3' mRNA Seq Library Prep FWD Kit for Illumina (Lexogen GmbH) (Moll *et al.*, 2014). All libraries were sequenced at 100 bp single-end reads using the Illumina system NextSeq1000. Raw reads were trimmed to 50 bp using Trim Galore (Martin, 2011) and mapped to the TAIR10 genome using the STAR aligner (Dobin et al., 2013) under the Lexogen recommended parameters. Differential expression between SA- and H_2O-treated samples was detected using DESeq2 (Love, Huber and Anders, 2014) with an adjusted p-value < 0.1 and a fold-change ≥ 2. GO Term Analysis was performed using PANTHER (Mi *et al.*, 2013) and *de novo* motif enrichment was uncovered using HOMER (Heinz et al., 2010) by analyzing promoters of differentially expressed genes from 1000 bp upstream to 200 bp downstream of the transcriptional start sites.

greenCUT&RUN

Six leaves from two plants were collected before and after treatment with 1 mM SA for 4 h and stored at -80 ºC. Frozen samples were ground to a fine powder and dissolved in 15 mL of the lysis buffer (20 mM Tris-HCl pH 7.5, 20% glycerol, 20 mM KCl, 2 mM EDTA, 2.5 mM

552 $MgCl_2$, 8.56% sucrose, and the protease inhibitor cocktail). Samples were filtered sequentially
553 through a 70-μm filter and a 40-μm filter before centrifuged at 1,500 x g at 4 ºC for 10 min. The
554 pellet was resuspended in the nuclei isolation buffer (20 mM Tris-HCl pH 7.5, 20% glycerol, 2.5
555 mM $MgCl_2$, 0.2% Triton X-100, and the protease inhibitor cocktail) and centrifuged at 1,500 x g
556 at 4 ºC for 10 min. The above resuspension and centrifugation steps were repeated 4x, until the
557 pellet was free of any green color. The pellet was resuspended in 1 mL of the greenCUT&RUN
558 wash buffer (20 mM HEPES-KOH pH 7.5, 150 mM NaCl, 0.5 mM Spermidine, and the protease
559 inhibitor cocktail). Isolated nuclei were then bound to 40 μL of Concanavalin A beads resuspended
560 in 10 μL of binding buffer (20 mM HEPES-KOH pH 7.5, 10 mM KCl, 1 mM $CaCl_2$, 1 mM $MnCl_2$,
561 and the protease inhibitor cocktail) and rotated for 10 min at room temperature. The beads were
562 collected using a magnetic rack, the supernatant was then removed, the bound nuclei were then
563 resuspended in 1 mL of the EDTA buffer (20 mM HEPES-KOH pH 7.5, 150 mM NaCl, 0.5 mM
564 Spermidine, 2 mM EDTA, and the protease inhibitor cocktail), and rotated at room temperature
565 for 10 min. The beads were collected again and resuspended in 100 μL of the greenCUT&RUN
566 wash buffer containing 10 μg/mL of nanobody-MNase (purified from *E. coli* strains carrying the
567 Addgene Plasmid #166035 through FPLC) and rotated at 4 °C for 30 min. After rotation, beads
568 were collected and washed twice in the greenCUT&RUN wash buffer. Beads were then put on ice,
569 resuspended in 150 μL of the calcium buffer (20 mM HEPES-KOH pH 7.5, 150 mM NaCl, 0.5
570 mM Spermidine, 3 mM $CaCl_2$, and the protease inhibitor cocktail) and incubated on ice for 30
571 min. After incubation, 100 μL of the 2X stop buffer (340 mM NaCl, 20 mM EDTA, 10 mM EGTA,
572 100 μg/mL RNase A, and 50 μg/mL Glycogen) was added to the beads and incubated at 37 °C for
573 30 min. After incubation, beads were removed, and the supernatant was collected for DNA
574 isolation. 2 μL of 10% SDS and 20 μg of Proteinase K were added to the collected supernatant

and incubated at 50 °C for 1 h. Equal volume of Phenol:Chloroform:Isoamyl Alcohol (25:24:1, v/v) was added to the samples followed by vortexing. The solution was transferred to a phase lock tube and centrifuged for 5 min at 16,000 x g at room temperature. After centrifugation, equal volume of chloroform was added, samples were inverted 10x, and centrifuged for 5 min at 16,000 x g at room temperature. The top aqueous layer was then taken and moved into new tubes containing 3 μL of 2 mg/mL of glycogen. 2x volumes of 100% ethanol was added to each sample to facilitate DNA precipitation overnight at -20 °C. After DNA precipitation, samples were centrifuged for 10 min at 16,000 x g at 4 °C. The supernatant was removed, the pellet was washed in 1 mL of 100% ethanol, and centrifuged for 5 min at 16,000 x g at 4 °C. The supernatant was removed, and the pellet was air dried for 5 to 10 min. The pellet was resuspended in 50 μL of H_2O and used for library preparation. The full protocol is available in the supplemental information.

CUT&RUN

Nuclei isolation for the CUT&RUN protocol was the same as for greenCUT&RUN described above. After nuclei isolation, the previously reported CUT&RUN protocol (Skene and Henikoff, 2017) was followed.

Construction and sequencing of greenCUT&RUN and CUT&RUN library

greenCUT&RUN and CUT&RUN libraries were constructed using the KAPA HyperPrep Kit (Roche Holding AG), with minor modifications. Briefly, end repair and A-tailing were performed at 20 °C for 30 min followed by deactivation of the A-tailing enzyme at 58 °C for 1 h. 1/100 diluted Illumina TruSeq DNA UD Indexes were ligated on to A-tailed DNA at 20 °C for 30 min. Post-ligation cleanup was performed twice, first using 1x library volume of AMPure Beads,

598 next with 1.2x library volume of AMPure Beads, followed by a double-sided size selection to
599 remove larger DNA fragments and smaller adapter dimers, respectively, using 0.7X-1.2X library
600 volume of AMPure Beads following the manufacture's protocol (Roche Holding AG). Ligated
601 libraries were then amplified using PCR and cleaned up twice with 1.2x library volume of AMPure
602 Beads to generate final purified libraries. Library size and concentration were determined using
603 Agilent 2100 Bioanalyzer and Qubit (Thermo Fisher Scientific), respectively. The *35S:NPR1-*
604 *GFP*, *35S:npr1^{rdr3}-GFP*, *35S:WRKY70-GFP*, and *35S:GFP* (control) libraries were sequenced at
605 75 bp paired-end reads using the Illumina system NextSeq500. The *BRM:BRM-GFP* and *35S:GFP*
606 (control) libraries were sequenced at 100 bp paired-end reads using the Illumina system
607 NextSeq1000.
608
609 **CUT&RUN and greenCUT&RUN data analysis**
610 Raw reads were trimmed using Trim Galore (Martin, 2011) and aligned to the TAIR10
611 genome using bowtie2 (Langmead and Salzberg, 2012). Concordant read Sequence Alignment
612 Map (SAM) files were converted to Binary Alignment Map (BAM) files and PCR-duplicated reads
613 were removed using SAMtools (Li et al., 2009). Deduplicated BAM files were then used to call
614 peaks using MACS2 (Zhang et al., 2008). Peaks called in all samples were used for further
615 analysis. Bigwig and bedgraph files of normalized Read Per Genomic Content (RPGC) were
616 generated using bamCoverage from deepTools 3.5.1 (Ramirez et al., 2014). Bigwig files were
617 visualized in IGV (Robinson et al., 2011). Normalized bigwig files and deepTools 3.5.1 were used
618 for generating Pearson correlation heatmaps, principal component analysis plots, and peak
619 heatmaps. *De novo* motif prediction of reproducible peaks was performed using HOMER (Heinz
620 *et al.*, 2010). GO Term Analysis was performed using PANTHER (Mi *et al.*, 2013). Cut frequency

plot was generated using cut-frequency (Nizamuddin *et al.*, 2021). Mean profile plots were generated using custom code in R.

Yeast two-hybrid

AH109 and Y187 yeast strains were transformed with the TGA/pGADT7 and NPR1/pGBKT7 constructs, respectively. NPR1 and npr1^{rdr3} were used as the bait and TGA3 and TGA5 were used as the prey. All protocols were carried out according to Clontech Yeast Protocols Handbook.

Protein analysis and immunoprecipitation (IP)

Protein analysis and IP were performed as previously described (Du et al., 2013). Briefly, recombinant proteins were transiently overexpressed in *N. benthamiana* by coinjecting the *Agrobacterium tumefaciens* strain GV3101 carrying the *35S:NPR1-GFP* construct ($OD_{600\ nm}$ = 0.5) or *35S:npr1^{rdr3}-GFP* construct ($OD_{600\ nm}$ = 0.5) with the *Agrobacterium tumefaciens* strain GV3101 carrying the *35S:TGA3-HA* or *35S:TGA5-HA* construct ($OD_{600\ nm}$ = 0.5) into the abaxial side of the leaf. After 44 h, plants were sprayed with 1 mM SA for 4 h before 1 g of tissue was collected and flash frozen. Frozen tissue was then ground and resuspended in 2.5 mL of the IP Buffer (10% glycerol, 25 mM Tris-HCl pH 7.5, 150 mM NaCl, 10 mM DTT, the protease inhibitor cocktail, and 0.2% NP-40). 40 μL of α-GFP beads (Chromotek) were added to the lysate for protein binding overnight at 4 °C, followed by 3x washes in the IP buffer. 50 μL of 4x LDS Sample Buffer (Thermo Fisher Scientific) was added to the beads and incubated at 70 °C for 20 min. Samples were then run on a 4-12% Bis-Tris gel and transferred to a membrane for western blotting

using α-GFP (Clontech) and α-HA (Cell Signaling Technology) antibodies. Band intensity was measured using the iBright Analysis Software (Thermo Fisher Scientific).

Statistics and reproducibility

For all statistical data, the center values are the mean, and the error bars represent the standard error of the mean except for Figure 4 qPCR data (standard deviation). All experiments were performed three or more times with similar results except the Affinity Purification LC-MS/MS, QuantSeq, and greenCUT&RUN, where one experiment with multiple biological replicates was performed.

Data Availability

The greenCUT&RUN, CUT&RUN, and QuantSeq sequencing data are available through the National Center for Biotechnology Information (NCBI) under the accession number PRJNA1050222. The mass spectrometry proteomics data have been deposited to the ProteomeXchange Consortium via the PRIDE (Perez-Riverol et al., 2022) partner repository with the dataset identifier PXD047543. Code generated in this study is available on GitHub (https://github.com/jjp55).

FUNDING

This work was supported by grants from the National Institutes of Health (NIH) 1R35GM118036 and the Howard Hughes Medical Institute to X.D; NIH 5T32GM007754-40 to J.P., NIH R01GM135706 to S.-L.X. and its diversity supplement to support A.V.R, as well as the Carnegie endowment to the Carnegie mass spectrometry facility.

AUTHOR CONTRIBUTIONS

X.D. conceived and supervised this project. J.P. carried out all the TurboID, CUT&RUN, greenCUT&RUN, QuantSeq, and molecular genetic experiments and performed the associated computational analyses. X.Z. generated the NPR1-3xHA-TurboID construct, validated NPR1 proximal partners using BiFC, and quantified the interaction. A.R. and S.X. performed the LC-MS/MS of the TurboID samples. R.Z. carried out the marker gene expression analysis. R.O. and J.P. performed the co-IP between NPR1/rdr3 and TGA5 and the western blots examining NPR1-GFP and rdr3-GFP expression. J.P. and X.D. wrote the manuscript with input from all coauthors.

ACKNOWLEDGEMENTS

We thank Dr. Marc Timmers (University of Feiburg) for providing the GFP nanobody-fused MNase enzyme and the recombinant plasmid encoding the fusion protein; Dr. Zhi-Yong Wang (Carnegie Institution for Science) for the gift of the YFP-YFP-TurboID line; Dr. Chenlong Li (Sun Yat-sen University) for sharing the *BRM:BRM-GFP* line; Dr. Tetsuji Katutani (University of Tokyo) for sharing the *LDL3:LDL3-3xFLAG* and *ldl3-1* lines; and members of the Dong laboratory for helpful discussion of the project. We thank the Duke University School of Medicine for the

683 use of the Sequencing and Genomic Technologies Shared Resource for providing Next Generation
684 Sequencing services.
685
686 **DECLARATION OF INTERESTS**
687 X.D. is a founder of Upstream Biotechnology Inc. and a member of its scientific advisory board,
688 as well as a scientific advisory board member of Inari Agriculture Inc. and Aferna Bio. X.D. is an
689 advisory board member for Molecular Plant.
690
691 **MATERIALS & CORRESPONDENCE**
692 * Correspondence and material requests should be addressed to: xdong@duke.edu
693

REFERENCES

Bazett-Jones, D.P., Cote, J., Landel, C.C., Peterson, C.L., and Workman, J.L. (1999). The SWI/SNF complex creates loop domains in DNA and polynucleosome arrays and can disrupt DNA-histone contacts within these domains. Mol Cell Biol **19**:1470-1478. 10.1128/MCB.19.2.1470.

Cao, H., Bowling, S.A., Gordon, A.S., and Dong, X. (1994). Characterization of an Arabidopsis Mutant That Is Nonresponsive to Inducers of Systemic Acquired Resistance. Plant Cell **6**:1583-1592. 10.1105/tpc.6.11.1583.

Chen, J., Mohan, R., Zhang, Y., Li, M., Chen, H., Palmer, I.A., Chang, M., Qi, G., Spoel, S.H., Mengiste, T., et al. (2019). NPR1 promotes its own and target gene expression in plant defense by recruiting CDK8. Plant Physiol **181**:289-304. 10.1104/pp.19.00124.

Clough, S.J., and Bent, A.F. (1998). Floral dip: a simplified method for Agrobacterium-mediated transformation of Arabidopsis thaliana. Plant J **16**:735-743. 10.1046/j.1365-313x.1998.00343.x.

Delannoy, E., Batardiere, B., Pateyron, S., Soubigou-Taconnat, L., Chiquet, J., Colcombet, J., and Lang, J. (2023). Cell specialization and coordination in Arabidopsis leaves upon pathogenic attack revealed by scRNA-seq. Plant Commun **4**:100676. 10.1016/j.xplc.2023.100676.

Despres, C., DeLong, C., Glaze, S., Liu, E., and Fobert, P.R. (2000). The Arabidopsis NPR1/NIM1 protein enhances the DNA binding activity of a subgroup of the TGA family of bZIP transcription factors. Plant Cell **12**:279-290.

Ding, Y., Sun, T., Ao, K., Peng, Y., Zhang, Y., Li, X., and Zhang, Y. (2018). Opposite roles of salicylic acid receptors NPR1 and NPR3/NPR4 in transcriptional regulation of plant immunity. Cell **173**:1454-1467 e1415. 10.1016/j.cell.2018.03.044.

Dobin, A., Davis, C.A., Schlesinger, F., Drenkow, J., Zaleski, C., Jha, S., Batut, P., Chaisson, M., and Gingeras, T.R. (2013). STAR: ultrafast universal RNA-seq aligner. Bioinformatics **29**:15-21. 10.1093/bioinformatics/bts635.

Du, Y., Zhao, J., Chen, T., Liu, Q., Zhang, H., Wang, Y., Hong, Y., Xiao, F., Zhang, L., Shen, Q., and Liu, Y. (2013). Type I J-domain NbMIP1 proteins are required for both Tobacco mosaic virus infection and plant innate immunity. PLoS Pathog **9**:e1003659. 10.1371/journal.ppat.1003659.

Fu, Z.Q., Yan, S., Saleh, A., Wang, W., Ruble, J., Oka, N., Mohan, R., Spoel, S.H., Tada, Y., Zheng, N., and Dong, X. (2012). NPR3 and NPR4 are receptors for the immune signal salicylic acid in plants. Nature **486**:228-232. 10.1038/nature11162.

Heinz, S., Benner, C., Spann, N., Bertolino, E., Lin, Y.C., Laslo, P., Cheng, J.X., Murre, C., Singh, H., and Glass, C.K. (2010). Simple combinations of lineage-determining transcription factors prime cis-regulatory elements required for macrophage and B cell identities. Mol Cell **38**:576-589. 10.1016/j.molcel.2010.05.004.

Huang, P., Dong, Z., Guo, P., Zhang, X., Qiu, Y., Li, B., Wang, Y., and Guo, H. (2020). Salicylic Acid Suppresses Apical Hook Formation via NPR1-Mediated Repression of EIN3 and EIL1 in Arabidopsis. Plant Cell **32**:612-629. 10.1105/tpc.19.00658.

Huang, S., Zhu, S., Kumar, P., and MacMicking, J.D. (2021). A phase-separated nuclear GBPL circuit controls immunity in plants. Nature **594**:424-429. 10.1038/s41586-021-03572-6.

Jin, H., Choi, S.M., Kang, M.J., Yun, S.H., Kwon, D.J., Noh, Y.S., and Noh, B. (2018). Salicylic acid-induced transcriptional reprogramming by the HAC-NPR1-TGA histone acetyltransferase complex in Arabidopsis. Nucleic Acids Res **46**:11712-11725. 10.1093/nar/gky847.

Kagey, M.H., Newman, J.J., Bilodeau, S., Zhan, Y., Orlando, D.A., van Berkum, N.L., Ebmeier, C.C., Goossens, J., Rahl, P.B., Levine, S.S., et al. (2010). Mediator and cohesin connect gene expression and chromatin architecture. Nature **467**:430-435. 10.1038/nature09380.

Kalde, M., Barth, M., Somssich, I.E., and Lippok, B. (2003). Members of the Arabidopsis WRKY group III transcription factors are part of different plant defense signaling pathways. Mol Plant Microbe Interact **16**:295-305. 10.1094/MPMI.2003.16.4.295.

Kim, J.H., Castroverde, C.D.M., Huang, S., Li, C., Hilleary, R., Seroka, A., Sohrabi, R., Medina-Yerena, D., Huot, B., Wang, J., et al. (2022). Increasing the resilience of plant immunity to a warming climate. Nature **607**:339-344. 10.1038/s41586-022-04902-y.

Kim, T.W., Park, C.H., Hsu, C.C., Kim, Y.W., Ko, Y.W., Zhang, Z., Zhu, J.Y., Hsiao, Y.C., Branon, T., Kaasik, K., et al. (2023). Mapping the signaling network of BIN2 kinase using TurboID-mediated biotin labeling and phosphoproteomics. Plant Cell **35**:975-993. 10.1093/plcell/koad013.

Kinkema, M., Fan, W., and Dong, X. (2000). Nuclear localization of NPR1 is required for activation of PR gene expression. Plant Cell **12**:2339-2350. 10.1105/tpc.12.12.2339.

Koidl, S., and Timmers, H.T.M. (2021). greenCUT&RUN: efficient genomic profiling of GFP-tagged transcription factors and chromatin regulators. Curr Protoc **1**:e266. 10.1002/cpz1.266.

Kong, A.T., Leprevost, F.V., Avtonomov, D.M., Mellacheruvu, D., and Nesvizhskii, A.I. (2017). MSFragger: ultrafast and comprehensive peptide identification in mass spectrometry-based proteomics. Nat Methods **14**:513-520. 10.1038/nmeth.4256.

Kumar, S., Zavaliev, R., Wu, Q., Zhou, Y., Cheng, J., Dillard, L., Powers, J., Withers, J., Zhao, J., Guan, Z., et al. (2022). Structural basis of NPR1 in activating plant immunity. Nature **605**:561-566. 10.1038/s41586-022-04699-w.

Langmead, B., and Salzberg, S.L. (2012). Fast gapped-read alignment with Bowtie 2. Nat Methods **9**:357-359. 10.1038/nmeth.1923.

Li, C., Gu, L., Gao, L., Chen, C., Wei, C.Q., Qiu, Q., Chien, C.W., Wang, S., Jiang, L., Ai, L.F., et al. (2016). Concerted genomic targeting of H3K27 demethylase REF6 and chromatin-remodeling ATPase BRM in Arabidopsis. Nat Genet **48**:687-693. 10.1038/ng.3555.

Li, H., Handsaker, B., Wysoker, A., Fennell, T., Ruan, J., Homer, N., Marth, G., Abecasis, G., Durbin, R., and Genome Project Data Processing, S. (2009). The Sequence Alignment/Map format and SAMtools. Bioinformatics **25**:2078-2079. 10.1093/bioinformatics/btp352.

Li, J., Zhong, R., and Palva, E.T. (2017). WRKY70 and its homolog WRKY54 negatively modulate the cell wall-associated defenses to necrotrophic pathogens in Arabidopsis. PLoS One **12**:e0183731. 10.1371/journal.pone.0183731.

Li, M., Chen, H., Chen, J., Chang, M., Palmer, I.A., Gassmann, W., Liu, F., and Fu, Z.Q. (2018). TCP Transcription Factors Interact With NPR1 and Contribute Redundantly to Systemic Acquired Resistance. Front Plant Sci **9**:1153. 10.3389/fpls.2018.01153.

Liu, X., Sun, Y., Korner, C.J., Du, X., Vollmer, M.E., and Pajerowska-Mukhtar, K.M. (2015). Bacterial Leaf Infiltration Assay for Fine Characterization of Plant Defense Responses using the Arabidopsis thaliana-Pseudomonas syringae Pathosystem. J Vis Exp 10.3791/53364.

Love, M.I., Huber, W., and Anders, S. (2014). Moderated estimation of fold change and dispersion for RNA-seq data with DESeq2. Genome Biol **15**:550. 10.1186/s13059-014-0550-8.

Mair, A., Xu, S.L., Branon, T.C., Ting, A.Y., and Bergmann, D.C. (2019). Proximity labeling of protein complexes and cell-type-specific organellar proteomes in Arabidopsis enabled by TurboID. Elife **8**10.7554/eLife.47864.

Malamy, J., Carr, J.P., Klessig, D.F., and Raskin, I. (1990). Salicylic Acid: a likely endogenous signal in the resistance response of tobacco to viral infection. Science **250**:1002-1004. 10.1126/science.250.4983.1002.

Maleck, K., Levine, A., Eulgem, T., Morgan, A., Schmid, J., Lawton, K.A., Dangl, J.L., and Dietrich, R.A. (2000). The transcriptome of Arabidopsis thaliana during systemic acquired resistance. Nat Genet **26**:403-410. 10.1038/82521.

Mann, R., and Notani, D. (2023). Transcription factor condensates and signaling driven transcription. Nucleus **14**:2205758. 10.1080/19491034.2023.2205758.

Martin, M. (2011). Cutadapt removes adapter sequences from high-throughput sequencing reads. 2011 **17**:3. 10.14806/ej.17.1.200.

Meers, M.P., Janssens, D.H., and Henikoff, S. (2019). Pioneer factor-nucleosome binding events during differentiation are motif encoded. Mol Cell **75**:562-575 e565. 10.1016/j.molcel.2019.05.025.

Meers, M.P., Bryson, T.D., Henikoff, J.G., and Henikoff, S. (2019). Improved CUT&RUN chromatin profiling tools. Elife **8**10.7554/eLife.46314.

Metraux, J.P., Signer, H., Ryals, J., Ward, E., Wyss-Benz, M., Gaudin, J., Raschdorf, K., Schmid, E., Blum, W., and Inverardi, B. (1990). Increase in salicylic Acid at the onset of systemic acquired resistance in cucumber. Science **250**:1004-1006. 10.1126/science.250.4983.1004.

Mi, H., Muruganujan, A., Casagrande, J.T., and Thomas, P.D. (2013). Large-scale gene function analysis with the PANTHER classification system. Nat Protoc **8**:1551-1566. 10.1038/nprot.2013.092.

Moll, P., Ante, M., Seitz, A., and Reda, T. (2014). QuantSeq 3′ mRNA sequencing for RNA quantification. Nature Methods **11**:i-iii. 10.1038/nmeth.f.376.

Mori, S., Oya, S., Takahashi, M., Takashima, K., Inagaki, S., and Kakutani, T. (2023). Cotranscriptional demethylation induces global loss of H3K4me2 from active genes in Arabidopsis. EMBO J **42**:e113798. 10.15252/embj.2023113798.

Nizamuddin, S., Koidl, S., Bhuiyan, T., Werner, T.V., Biniossek, M.L., Bonvin, A., Lassmann, S., and Timmers, H. (2021). Integrating quantitative proteomics with accurate genome profiling of transcription factors by greenCUT&RUN. Nucleic Acids Res **49**:e49. 10.1093/nar/gkab038.

Nobori, T., Monell, A., Lee, T.A., Zhou, J., Nery, J., and Ecker, J.R. (2023). Time-resolved single-cell and spatial gene regulatory atlas of plants under pathogen attack. bioRxiv:2023.2004.2010.536170. 10.1101/2023.04.10.536170.

Nomoto, M., Skelly, M.J., Itaya, T., Mori, T., Suzuki, T., Matsushita, T., Tokizawa, M., Kuwata, K., Mori, H., Yamamoto, Y.Y., et al. (2021). Suppression of MYC transcription activators by the immune cofactor NPR1 fine-tunes plant immune responses. Cell Rep **37**:110125. 10.1016/j.celrep.2021.110125.

O'Malley, R.C., Huang, S.C., Song, L., Lewsey, M.G., Bartlett, A., Nery, J.R., Galli, M., Gallavotti, A., and Ecker, J.R. (2016). Cistrome and Epicistrome Features Shape the Regulatory DNA Landscape. Cell **165**:1280-1292. 10.1016/j.cell.2016.04.038.

Olate, E., Jimenez-Gomez, J.M., Holuigue, L., and Salinas, J. (2018). NPR1 mediates a novel regulatory pathway in cold acclimation by interacting with HSFA1 factors. Nat Plants **4**:811-823. 10.1038/s41477-018-0254-2.

Perez-Riverol, Y., Bai, J., Bandla, C., Garcia-Seisdedos, D., Hewapathirana, S., Kamatchinathan, S., Kundu, D.J., Prakash, A., Frericks-Zipper, A., Eisenacher, M., et al.

(2022). The PRIDE database resources in 2022: a hub for mass spectrometry-based proteomics evidences. Nucleic Acids Res **50**:D543-D552. 10.1093/nar/gkab1038.

Ramirez, F., Dundar, F., Diehl, S., Gruning, B.A., and Manke, T. (2014). deepTools: a flexible platform for exploring deep-sequencing data. Nucleic Acids Res **42**:W187-191. 10.1093/nar/gku365.

Rio, D.C., Ares, M., Jr., Hannon, G.J., and Nilsen, T.W. (2010). Purification of RNA using TRIzol (TRI reagent). Cold Spring Harb Protoc **2010**:pdb prot5439. 10.1101/pdb.prot5439.

Robinson, J.T., Thorvaldsdottir, H., Winckler, W., Guttman, M., Lander, E.S., Getz, G., and Mesirov, J.P. (2011). Integrative genomics viewer. Nat Biotechnol **29**:24-26. 10.1038/nbt.1754.

Saleh, A., Withers, J., Mohan, R., Marques, J., Gu, Y., Yan, S., Zavaliev, R., Nomoto, M., Tada, Y., and Dong, X. (2015). Posttranslational modifications of the master transcriptional regulator NPR1 enable dynamic but tight control of plant immune responses. Cell Host Microbe **18**:169-182. 10.1016/j.chom.2015.07.005.

Schneider, C.A., Rasband, W.S., and Eliceiri, K.W. (2012). NIH Image to ImageJ: 25 years of image analysis. Nat Methods **9**:671-675. 10.1038/nmeth.2089.

Seo, S.Y., Wi, S.J., and Park, K.Y. (2020). Functional switching of NPR1 between chloroplast and nucleus for adaptive response to salt stress. Sci Rep **10**:4339. 10.1038/s41598-020-61379-3.

Shannon, P., Markiel, A., Ozier, O., Baliga, N.S., Wang, J.T., Ramage, D., Amin, N., Schwikowski, B., and Ideker, T. (2003). Cytoscape: a software environment for integrated models of biomolecular interaction networks. Genome Res **13**:2498-2504. 10.1101/gr.1239303.

Singh, M., Bag, S.K., Bhardwaj, A., Ranjan, A., Mantri, S., Nigam, D., Sharma, Y.K., and Sawant, S.V. (2015). Global nucleosome positioning regulates salicylic acid mediated transcription in Arabidopsis thaliana. BMC Plant Biol **15**:13. 10.1186/s12870-014-0404-2.

Skene, P.J., and Henikoff, S. (2017). An efficient targeted nuclease strategy for high-resolution mapping of DNA binding sites. Elife **6**10.7554/eLife.21856.

Szklarczyk, D., Gable, A.L., Lyon, D., Junge, A., Wyder, S., Huerta-Cepas, J., Simonovic, M., Doncheva, N.T., Morris, J.H., Bork, P., et al. (2019). STRING v11: protein-protein association networks with increased coverage, supporting functional discovery in genome-wide experimental datasets. Nucleic Acids Res **47**:D607-D613. 10.1093/nar/gky1131.

Tang, Y., Ho, M.I., Kang, B.H., and Gu, Y. (2022). GBPL3 localizes to the nuclear pore complex and functionally connects the nuclear basket with the nucleoskeleton in plants. PLoS Biol **20**:e3001831. 10.1371/journal.pbio.3001831.

Tyanova, S., Temu, T., Sinitcyn, P., Carlson, A., Hein, M.Y., Geiger, T., Mann, M., and Cox, J. (2016). The Perseus computational platform for comprehensive analysis of (prote)omics data. Nat Methods **13**:731-740. 10.1038/nmeth.3901.

Wang, D., Amornsiripanitch, N., and Dong, X. (2006). A genomic approach to identify regulatory nodes in the transcriptional network of systemic acquired resistance in plants. PLoS Pathog **2**:e123. 10.1371/journal.ppat.0020123.

Wang, W., Withers, J., Li, H., Zwack, P.J., Rusnac, D.V., Shi, H., Liu, L., Yan, S., Hinds, T.R., Guttman, M., et al. (2020). Structural basis of salicylic acid perception by Arabidopsis NPR proteins. Nature **586**:311-316. 10.1038/s41586-020-2596-y.

Weigel, R.R., Pfitzner, U.M., and Gatz, C. (2005). Interaction of NIMIN1 with NPR1 modulates PR gene expression in Arabidopsis. Plant Cell **17**:1279-1291. 10.1105/tpc.104.027441.

Wickham, H. (2016). ggplot2: elegant graphics for data analysis (Springer-Verlag New York).

Wu, Y., Zhang, D., Chu, J.Y., Boyle, P., Wang, Y., Brindle, I.D., De Luca, V., and Despres, C. (2012). The Arabidopsis NPR1 protein is a receptor for the plant defense hormone salicylic acid. Cell Rep **1**:639-647. 10.1016/j.celrep.2012.05.008.

Xu, S.L., Shrestha, R., Karunadasa, S.S., and Xie, P.Q. (2023). Proximity Labeling in Plants. Annu Rev Plant Biol **74**:285-312. 10.1146/annurev-arplant-070522-052132.

Xu, X., Chen, C., Fan, B., and Chen, Z. (2006). Physical and functional interactions between pathogen-induced Arabidopsis WRKY18, WRKY40, and WRKY60 transcription factors. Plant Cell **18**:1310-1326. 10.1105/tpc.105.037523.

Yun, S.H., Khan, I.U., Noh, B., and Noh, Y.S. (2024). Genomic overview of INA-induced NPR1 targeting and transcriptional cascades in Arabidopsis. Nucleic Acids Res 10.1093/nar/gkae019.

Zavaliev, R., Mohan, R., Chen, T., and Dong, X. (2020). Formation of NPR1 condensates promotes cell survival during the plant immune response. Cell **182**:1093-1108 e1018. 10.1016/j.cell.2020.07.016.

Zhang, X., Yao, J., Zhang, Y., Sun, Y., and Mou, Z. (2013). The Arabidopsis Mediator complex subunits MED14/SWP and MED16/SFR6/IEN1 differentially regulate defense gene expression in plant immune responses. Plant J **75**:484-497. 10.1111/tpj.12216.

Zhang, Y., Fan, W., Kinkema, M., Li, X., and Dong, X. (1999). Interaction of NPR1 with basic leucine zipper protein transcription factors that bind sequences required for salicylic acid induction of the PR-1 gene. Proc Natl Acad Sci U S A **96**:6523-6528. 10.1073/pnas.96.11.6523.

Zhang, Y., Liu, T., Meyer, C.A., Eeckhoute, J., Johnson, D.S., Bernstein, B.E., Nusbaum, C., Myers, R.M., Brown, M., Li, W., and Liu, X.S. (2008). Model-based analysis of ChIP-Seq (MACS). Genome Biol **9**:R137. 10.1186/gb-2008-9-9-r137.

Zheng, X.Y., and Gehring, M. (2019). Low-input chromatin profiling in Arabidopsis endosperm using CUT&RUN. Plant Reprod **32**:63-75. 10.1007/s00497-018-00358-1.

Zhou, J.M., Trifa, Y., Silva, H., Pontier, D., Lam, E., Shah, J., and Klessig, D.F. (2000). NPR1 differentially interacts with members of the TGA/OBF family of transcription factors that bind an element of the PR-1 gene required for induction by salicylic acid. Mol Plant Microbe Interact **13**:191-202. 10.1094/MPMI.2000.13.2.191.

Zhu, J., Lolle, S., Tang, A., Guel, B., Kvitko, B., Cole, B., and Coaker, G. (2023). Single-cell profiling of Arabidopsis leaves to Pseudomonas syringae infection. Cell Rep **42**:112676. 10.1016/j.celrep.2023.112676.

Zhu, W., Smith, J.W., and Huang, C.M. (2010). Mass spectrometry-based label-free quantitative proteomics. J Biomed Biotechnol **2010**:840518. 10.1155/2010/840518.

FIGURES AND FIGURE LEGENDS

Figure 1. NPR1-proxiome contains transcriptional machineries and chromatin remodelers shared by GBPL3-proxiome. (A) Volcano plot of NPR1 proximal proteins 4 h after SA treatment detected through TurboID biotin affinity purification followed by Label Free Quantification (LFQ) Mass Spectrometry processed under mild conditions (see Methods). Red points represent proteins that have an $NPR1_{LFQ}/YFP_{LFQ} \geq 2$ and p-value < 0.1 in both mild and harsh washing conditions (see Methods) or p-value < 0.01 in at least one washing condition. The single blue point (on the right) represents NPR1. **(B)** Log_2(Maximum LFQ Intensity) of NPR1-3xHA-TbID, YFP-YFP-TbID (BAIT), and known NPR1 interactors in NPR1-3xHA-TbID (NPR1) vs. YFP-YFP-TbID (YFP) samples. **(C)** Venn diagram comparing NPR1 proximal proteins identified in the current TurboID experiment with those identified in the cytoplasmic SA-induced NPR1 condensates (cSINCs) (Zavaliev *et al.*, 2020). **(D)** Enriched molecular functions (MF) of the 234 NPR1 proximal proteins. **(E)** Proximity between NPR1 and LDL3 or BRM. nYFP-fused NPR1 (NPR1-YN) and cYFP-fused BRM C-terminus (amino acids 953-2193) (BRM.C-YC) or cYFP-fused LDL3 (LDL3-YC), were co-expressed with the nuclear marker protein Histone 2B fused to mCherry (HTB1-mCherry) in *N. benthamiana*. Plants were imaged after treatment with water (Mock) or 1 mM SA for 8 h and the BiFC intensities were measured from multiple nuclei and values were plotted on a Box and whiskers plot. Different letters indicate statistical significance based on an ordinary one-way ANOVA with Tukey's multiple comparisons tests (a single pooled variance). Asterisks indicate statistical significance tested by two-tailed unpaired Student's t-test (****, P<0.0001). Scale bar =10 μm. **(F and G)** WT, *npr1-2*, *brm-3*, *BRM:BRM-GFP/brm-1* (**F**), *ldl3-1*, *ldl3-2*, and *LDL3-FLAG/ldl3-1* (**G**) treated with H_2O (Mock) or 1 mM SA for 24 h prior to

inoculation with *Psm* ES4326 at $OD_{600\ nm}$ = 0.001. Bacterial colony-forming units (cfu) were measured 3 days post inoculation (n = 8; error bars represent SEM; two-sided t-test and two-way ANOVA were used for comparisons within and between genotypes, respectively). **(H)** STRING network analysis (Szklarczyk *et al.*, 2019) of NPR1 proximal proteins relating to chromatin remodeling and transcriptional regulation. Blue shade, proteins shared with GBPL3-proxiome (Tang *et al.*, 2022).

Figure 2. NPR1 targets TF gene promoters through association with TGA TFs. (A) Pearson's correlation of the greenCUT&RUN data from plants expressing NPR1-GFP (NPR1) and GFP with and without 1 mM SA treatment for 4 h. **(B)** Integrative Genomics Viewer (IGV) of the *PR1* promoter showing normalized NPR1-GFP and GFP binding before and after SA treatment. **(C)** Mean profile of Reads Per Genomic Content (RPGC) of NPR1-GFP reads before and after SA treatment at NPR1-target genes. TSS, transcriptional start site. **(D)** Motifs enriched under NPR1-GFP peaks 4 h after 1 mM SA treatment. **(E)** Cut frequency of all *as-1* elements (TGACG) by the GFP nanobody-MNase in the overall NPR1-GFP peaks 4 h after 1 mM SA treatment. **(F)** The enriched biological processes (BP) and molecular functions (MF) of NPR1-target genes. **(G)** Venn diagram displaying shared NPR1 loci 1, 2, 4, 8, and 24 h after 1 mM SA treatment. **(H)** Heatmaps and mean profile of normalized (RPGC) NPR1 binding at shared loci (outlined in blue) and unique loci (outlined in green) 1, 2, 4, 8, and 24 h after 1 mM SA treatment. (**(I)** Mean profile of Reads Per Genomic Content (RPGC) of NPR1-GFP and npr1^{sim3}-GFP (sim3) before and after SA treatment at NPR1-target genes. TSS, transcriptional start site.

Figure 3. WRKY54/70 are major TFs downstream of NPR1-TGA that positively regulate SA-mediated gene expression and resistance. (A) Mean profile of Reads Per Genomic Content (RPGC) of WRKY70-GFP (WRKY70) and GFP reads of WRKY70-target genes. TSS, transcriptional start site. **(B)** Motifs enriched under WRKY70-GFP peaks. **(C)** Enriched biological processes (BP) and molecular functions (MF) of WRKY70-target genes. **(D)** Venn diagram illustrating the overlap between NPR1- and WRKY70-target genes. **(E and F)** Integrative Genomics Viewer (IGV) of normalized NPR1 and WRKY70 binding at the promoters of their shared target genes *WRKY63* (**E**) and *PCR1* (**F**). (**G**) RPGC of NPR1-GFP and WRKY70-GFP at 116 shared target genes 1 kb upstream and downstream of NPR1 peaks. **(H)** RPGC of all NPR1-GFP and WRKY70-GFP target genes centered on their respective peaks. **(I)** Correlation between SA-induced transcription and NPR1-dependency in WRKY70-target genes. r, Pearson correlation coefficient. **(J)** Correlation between SA-induced transcription and WRKY54/70-dependency in NPR1-target genes. **(K)** Bacterial colony-forming units (cfu) in WT, *wrky54/70*, and *npr1-2*. Plants were treated with H_2O (Mock) or 1 mM SA for 24 h before being inoculated with *Psm* ES4326 at $OD_{600\ nm}$ = 0.001. CFUs were measured 2 days post inoculation (n = 8; error bars represent SEM; two-sided t-test and two-way ANOVA were used for comparison within and between genotypes, respectively).

Figure 4. Biomolecular condensate formation stabilizes NPR1 association with TGA TF and enhances its transcriptional activity. (A) Mean profile of Reads Per Genomic Content (RPGC) of NPR1-GFP (NPR1) and npr1^{rdr3}-GFP (rdr3) at NPR1-target genes before and after 4 h of 1 mM SA treatment. TSS, transcriptional start site. **(B and C)** co-immunoprecipitation (co-IP) between TGA3 (**B**) or TGA5 (**C**) and NPR1 or rdr3 transiently overexpressed in *N. benthamiana*. Value under the IP blot represents band intensities normalized to TGA TF input. **(D)** Quantification of normalized co-IP TGA3-HA or TGA5-HA band intensity from three independent replicates (n = 3, error bars represent SEM, two-sided t-test was used for comparison between NPR1 and rdr3). **(E)** Interaction between TGA3 or TGA5 fused to the activator domain (AD) and NPR1 or rdr3 fused to the DNA-binding domain (BD) in the yeast two-hybrid assay. Yeast strains were mated for 24 h, normalized to $OD_{600\ nm}$ = 1.0, serially diluted, and plated on the indicated Synthetic Defined (SD) media without leucine and tryptophan (LW) or without leucine, tryptophan, histidine, and adenine (LWHA), and incubated at 30 °C. Photos were taken 2 days after plating. **(F)** Protein level of NPR1-GFP and rdr3-GFP in stable transgenic *Arabidopsis* plants. **(G-J)** Transcript levels of *NPR1* or *rdr3* (**G**) and target genes *PR1* (**H**), *WRKY18* (**I**), and *WRKY70* (**J**) in *35S:NPR1-GFP/npr1-2*, *35S:npr1^{rdr3}-GFP/npr1-2*, and *npr1-2* plants measured using qPCR 8 h after SA induction (n = 3, error bars represent standard deviation). **(K-N)** Mean profile of Reads Per Genomic Content (RPGC) of BRM-GFP reads at BRM-target genes (**K**), NPR1-target genes (**L**), WRKY70-target genes **(M)**, and SA-induced genes **(N)** 4 h after treatment with H_2O or 1 mM SA. TSS, transcriptional start site. **(O)** Working model of the SA/NPR1 signaling hub and transcriptional cascade. Overlapped rectangular shades show that NPR1- and GBPL3-condensates share general transcriptional regulatory machineries (e.g., Mediator, SWI/SNF, and histone

993 modifiers), but target different genes through association with unique TFs. An increase in SA level
994 triggers the transcriptional cascade by first activating NPR1 to induce TGA-mediated expression
995 of WRKY, MYB, NAC and ERF TFs which in turn activate the subsequent gene expression.